




## Article

# Electrochemical Behavior of Pt–Ru Catalysts Supported on Graphitized Ordered Mesoporous Carbons toward CO and Methanol Oxidation

Juan Carlos Calderón Gómez <sup>1,\*</sup>, Verónica Celorrio <sup>2,3</sup> , Laura Calvillo <sup>4</sup>, David Sebastián <sup>1</sup> , Rafael Moliner <sup>1</sup> and María Jesús Lázaro Elorri <sup>1,\*</sup> 

<sup>1</sup> Instituto de Carboquímica (CSIC), Miguel Luesma Castán 4, 50018 Zaragoza, Spain; dsebastian@icb.csic.es (D.S.); rmoliner@icb.csic.es (R.M.)

<sup>2</sup> UK Catalysis Hub, Research Complex at Harwell, RAL, Oxford OX11 0FA, UK; v.celorrio@ucl.ac.uk

<sup>3</sup> Kathleen Lonsdale Building, Department of Chemistry, University College London, Gordon Street, London WC1H 0AJ, UK

<sup>4</sup> Dipartimento di Scienze Chimiche, Università di Padova, Via Marzolo 1, 35131 Padova, Italy; laura.calvillolamano@unipd.it

\* Correspondence: jccalderon@icb.csic.es (J.C.C.G.); mlazaro@icb.csic.es (M.J.L.E.); Tel.: +34-976-733-977 (J.C.C.G. & M.J.L.E.)

Received: 29 November 2018; Accepted: 27 December 2018; Published: 3 January 2019



**Abstract:** In this work, graphitized ordered mesoporous carbons (gCMK-3) were employed as support for Pt and Pt–Ru nanoparticles synthesized by different reduction methods. The catalysts displayed metal contents and Pt:Ru atomic ratios close to 20 wt % and 1:1, respectively. A comparison of the physical parameters of Pt and Pt–Ru catalysts demonstrated that Ru enters into the Pt crystal structure, with well-dispersed nanoparticles on the carbon support. The Pt catalysts exhibited similar surface oxide composition, whereas a variable content of surface Pt and Ru oxides was found for the Pt–Ru catalysts. As expected, the Pt–Ru catalysts showed low CO oxidation onset and peak potentials, which were attributed to the high relative abundances of both metallic Pt and Ru oxides. All the studied catalysts exhibited higher maximum current densities than those observed for the commercial Pt and Pt–Ru catalysts, although the current–time curves at 0.6 V vs. reversible hydrogen electrode (RHE) demonstrated a slightly higher stationary current density in the case of the Pt/C commercial catalyst compared with Pt nanoparticles supported on gCMK-3s. However, the stationary currents obtained from the Pt–Ru/gCMK-3 catalysts surpassed those of the commercial Pt–Ru material, suggesting the suitability of the prepared catalysts as anodes for these devices.

**Keywords:** Pt–Ru catalysts; ordered mesoporous carbons; graphitization; CO oxidation; methanol oxidation; direct methanol fuel cells

## 1. Introduction

A quite interesting carbon material used as support for electrodes in direct methanol fuel cells (DMFCs) is the ordered mesoporous carbon (OMC). This material is synthesized by nanocasting using a silica template, which is impregnated with a carbon-based resin that, after carbonization and silica removal, results in an OMC with a 3D interconnected porous structure, high surface area, and rich content of mesopores [1], which promote the formation of uniformly distributed nanoparticles on the carbon surface [2]. Moreover, it is possible to modify its surface chemistry by creating surface functional groups that act as anchoring sites and enhance the electronic transfer between the catalytic nanoparticles and the support. The challenge is to maintain the ordered structure during the functionalization treatments in order to preserve the mesoporous structure as well as the high

surface area [3,4], which has been demonstrated to be crucial for the performance of OMC-supported Pt nanoparticles [5,6].

Despite the mentioned outstanding properties of OMCs, their low electrical conductivity hinders their use in fuel cells. The relatively low temperatures employed during the carbonization stage seem to be the cause for the poor formation of extensive graphite layers [7,8]. To avoid this drawback, graphitization of OMCs has been suggested by means of different procedures, such as the use of aromatic and polyaromatic hydrocarbons as carbon precursors during the silica template impregnation, as they can produce more graphitic domains after carbonization. Some of these organic molecules could be benzene, naphthalene, anthracene, and pyrene [9]. A similar procedure indicated that Fe phthalocyanines can also generate graphitic planes, but this methodology is expensive due to the high cost of these molecules, even when low temperatures are used for carbonization [10]. Postsynthesis heat treatments are accepted as a useful way to obtain graphitized OMCs, although part of the ordered structure can be altered, broadening the pore size distribution [11]. Some of these treatments can be performed at temperatures lower than 1000 °C in the presence of transition metal salts [12–14] or increasing the temperature until 1500 °C in N<sub>2</sub> or Ar atmosphere, avoiding the use of these metal compounds.

Graphitized OMCs have been employed to support Pt nanoparticles, finding enhanced stationary current densities for the oxidation of methanol compared with other Pt catalysts supported on carbon nanofibers, carbon nanocoils, and carbon black [6]. Pd nanoparticles have also been supported on these materials to test their viability as anode catalysts in formic acid fuel cells. The current densities associated with the oxidation of formic acid on these catalysts were higher than those observed on a Pd catalyst supported on carbon black [15]. Regarding their use as cathode supports, Rivera et al. prepared Pt<sub>2</sub>CrCo alloys supported on graphitized OMCs to assess the oxygen reduction reaction (ORR) on them. The authors obtained materials with outstanding activity toward the ORR, even in the presence of methanol, considering the crossover of this fuel between the anode and the cathode in DMFCs [16].

In this work, the activity of Pt and Pt–Ru catalysts supported on different graphitized ordered mesoporous carbon (gCMK-3) was studied in order to determine their behavior toward the CO and methanol electro-oxidation. It is important to highlight that the activity of Pt–Ru catalysts supported on graphitized ordered mesoporous carbons toward the mentioned molecules have not been reported in the literature, whereas the state of the art related to the behavior and performance of Pt catalysts supported on graphitized ordered mesoporous carbons toward the methanol electrochemical oxidation is in an incipient state. The CMK-3 was prepared using different TEOS/P123 mass ratios and subsequently treated at 1500 °C in Ar atmosphere to induce the formation of graphitic planes [6,15,16]. The Pt and Pt–Ru catalysts were prepared employing different reducing agents to verify their influence on the physical and electrochemical behavior of the catalysts. The gCMK-3-supported catalysts displayed higher CO tolerance and improved methanol oxidation current densities than those observed for commercial Pt and Pt–Ru catalysts supported on carbon black from E-TEK, which were used as reference to evaluate the results displayed for these catalysts.

## 2. Materials and Methods

### 2.1. Synthesis of Graphitized Ordered Mesoporous Carbon (gCMK)

CMK-3 was prepared by an incipient wetness impregnation procedure as described in Reference [15]. Briefly, the SBA-15 silica (Sigma-Aldrich, Madrid, Spain) was impregnated with the carbon precursor (furan resin, Huttenes-Albertus, Düsseldorf, Germany). The volume of furan resin used in the synthesis was equal to the silica porous volume ( $\sim 1 \text{ cm}^3 \text{ g}^{-1}$ ). After letting the material dry, it was subjected to a thermal treatment in nitrogen atmosphere at 700 °C for 2 h, and the silica was then removed using HF (40%, Fluka, Bucharest, Romania). Two silica templates with different textural properties were used for the synthesis. They were prepared by following the procedure described in

Reference [17] and using a TEOS/P123 (Sigma-Aldrich, Madrid, Spain) mass ratio (R) equal to 2 and 8 (SBA-15/R2 and SBA-15/R8, respectively). The carbon supports derived from these silica materials were labeled as CMK-3-R2 and CMK-3-R8 [17,18]. Finally, the CMK-3 materials were heat-treated at 1500 °C in a graphite electrical furnace for 1 h under argon flow in order to obtain the graphitized material (gCMK-3) [15].

## 2.2. Synthesis of gCMK-3-Supported Pt and Pt–Ru Catalysts

Pt and Pt–Ru catalysts supported on gCMK-3s were synthesized employing three different procedures described below. In all methods, a solution of the metal precursor salts ( $\text{H}_2\text{PtCl}_6$  8% w/w solution and  $\text{RuCl}_3$ , 99.999%, Sigma-Aldrich, Madrid, Spain) was prepared in water or ethylene glycol (Sigma-Aldrich, Madrid, Spain) in order to obtain materials with a Pt:Ru atomic ratio of 1:1.

Method 1 (sodium borohydride method, BM): gCMK-3 was dispersed in water, and the solution containing the metal precursors was then slowly added under vigorous stirring. Finally, a 26.4 mM sodium borohydride (Sigma-Aldrich, Madrid, Spain) solution was added dropwise under sonication [3].

Method 2 (formic acid method, FAM): gCMK-3 was dispersed in a 2 M formic acid (Merck, Darmstadt, Germany) solution and then heated at 80 °C. Afterward, the metal precursor solution was slowly added and kept at this temperature for 12 h [4].

Method 3 (ethylene glycol method, EG): the metal precursors and the carbon support were dispersed in EG, and the pH was adjusted to 11 using a NaOH (Sigma-Aldrich, Madrid, Spain) solution in EG. The dispersion was heated at 195 °C for 2 h, quickly cooled down to room temperature, and the pH adjusted to 1 with HCl (Merck, Darmstadt, Germany) [19].

Finally, all the materials were filtered, washed, and dried at 60 °C. The catalyst were labeled as Pt/gCMK-3-RX-Y or Pt–Ru/gCMK-3-RX-Y, with X = 2, 8 and Y = BM, FAM, EG.

## 2.3. Physicochemical Characterization of the Catalysts

Energy dispersive X-ray (EDX) was employed to determine the metal content of the synthesized catalysts using a scanning electron microscope (SEM) Hitachi S-3400N (Hitachi, Düsseldorf, Germany) coupled to a Röntec XFlash analyzer (RÖNTEC GmbH, Berlin, Germany). This instrument is equipped with a Be window and a Si(Li) detector (Hitachi, Düsseldorf, Germany) operating at 15 keV.

X-ray diffraction (XRD) analyses were carried out to study the crystalline properties of the catalysts. XRD patterns were obtained by means of a Bruker AXS D8 Advance diffractometer (Bruker, Karlsruhe, Deutschland), with a  $\theta$ - $\theta$  configuration and a Cu-K $\alpha$  radiation ( $\lambda = 0.154$  nm). The scans were achieved between 0° and 100° for  $2\theta$  values. The (220) peak located at  $2\theta \approx 70^\circ$  and the Scherrer's equation were used to calculate the crystallite size [20].

X-ray photoelectron spectroscopy (XPS) analysis was performed in order to determine the chemical state and the surface composition of Pt and Ru in the catalysts. An ESCAPlus Omicron spectrometer (Omicron, Houston, TX, USA) equipped with a concentric hemispherical analyzer, seven channeltron detectors, and an Al/Mg monochromated X-ray source ( $K\alpha = 1253.6$  eV) was employed. This equipment was operated at 15 kV and 15 mA. The XPS spectra were recorded at pressures lower than  $8 \times 10^{-9}$  mbar. Data processing was performed with the CASAXPS<sup>®</sup> software (SurfaceSpectra, Manchester, UK), fitting the experimental data with Gaussian–Lorentzian curves.

In order to determine the particle size and the dispersion of the nanoparticles on the gCMK-3s, transmission electron microscopy (TEM) analyses were made using a 200 kV JEOL-2000 FXII transmission electron microscope (JEOL, Peabody, MA, USA). The catalysts were dropped from an ethanol suspension on a carbon grid. The images were taken with a MultiScan CCD Gatan 694 (Gatan, Pleasanton, CA, USA) camera and treated with the ImageJ<sup>®</sup> software (National Institutes for Health, Bethesda, MD, USA).

## 2.4. Electrochemical Characterization

A three-electrode cell connected to an AUTOLAB NS85630 modular equipment (Metrohm, Herisau, Switzerland) was employed to assess the electrochemical activity of the synthesized materials. A reversible hydrogen electrode (RHE) placed inside a Luggin capillary was used as the reference electrode, and a glassy carbon bar was used as the counter electrode. A catalyst-modified glassy carbon disk was used as the working electrode. The catalyst inks were prepared with 2.0 mg of catalyst, 15 mL of Nafion<sup>®</sup> (5 wt %, Sigma-Aldrich, Madrid, Spain) and 500 mL of ultrapure water. Afterward, a 60- $\mu$ L aliquot was deposited and dried on the glassy carbon disk. All the aqueous solutions were prepared with high resistivity deoxygenated 18.2 M $\Omega$  cm H<sub>2</sub>O. 0.5 M H<sub>2</sub>SO<sub>4</sub> (95%–97%, Merck, Darmstadt, Germany) was used as the supporting electrolyte. For the methanol electrochemical characterization, 2.0 M methanol (99%, Merck, Darmstadt, Germany) solutions in the supporting electrolyte were employed. CO activity was studied by bubbling CO (99.999%, Air Liquide, Madrid, Spain) into the electrochemical cell for 10 min at 0.2 V vs. RHE and 20 °C in order to form a CO monolayer on the deposited catalyst; then, nitrogen (MicroGen2, GasLab, Fremont, CA, USA) was bubbled for 20 min to remove the dissolved CO from the supporting electrolyte. Two potential scans at 0.020 V s<sup>−1</sup> between 0.05 V and 1.0 V vs. RHE were applied. All the experiments were performed at 20 °C, while all the current densities presented in this paper have been normalized by the electroactive area calculated from the charge associated with the oxidation of an adsorbed CO monolayer on Pt (420  $\mu$ C cm<sup>−2</sup><sub>Pt</sub>).

The results obtained from the physical and the electrochemical characterization were compared against those exhibited by the commercial Pt and Pt–Ru catalysts supported on carbon black from E-TEK (DeNora, Milan, Italy). These catalysts have a metal content close to 20 wt% and a Pt:Ru ratio near 1:1.

## 3. Results

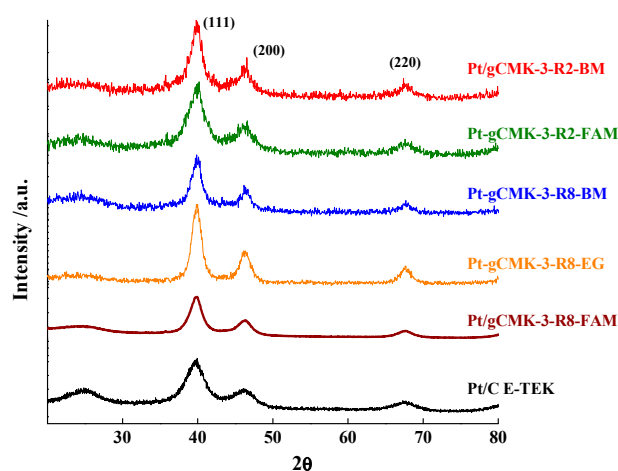
### 3.1. Physical Characterization

Table 1 summarizes the metal content of the different studied catalysts. In all the cases, metal contents around 20 wt% were observed, agreeing with the nominal values. Pt:Ru atomic ratios were close to 1:1, except in the case of the catalyst prepared by the EG method, which exhibited a higher Pt atomic content (66%).

Figures 1 and 2 depict the XRD patterns for the prepared Pt and Pt–Ru catalysts, respectively. All the catalysts presented the typical (110), (200), and (220) peaks for the face-centered cubic structure of Pt located at  $2\theta$  of 39.75°, 46.31°, and 67.48°, as those observed for the commercial Pt/C and Pt–Ru/C. On the other hand, the peaks for the Pt–Ru materials exhibited a shift toward higher  $2\theta$  values with respect to those of the Pt catalysts (see Figure 2), which is attributed to the structure contraction due to the incorporation of Ru into the fcc Pt crystalline structure [21–23]. This fact was corroborated by the smaller lattice parameter calculated for the Pt–Ru materials compared with the Pt values (see Table 1). Furthermore, a peak around 25° in the XRD patterns of the Pt and Pt–Ru commercial catalysts was detected, which corresponds to the (002) reflection of the graphite basal planes present in the carbon black acting as support for these materials.

**Table 1.** Physical characterization of the catalysts supported on graphitized ordered mesoporous carbons (gCMK-3s) and the commercial Pt/C E-TEK. Metal surface area:  $SA \text{ (m}^2 \text{ g}^{-1}\text{)} = 6 \times 10^3 / \rho d$ , with  $d$  as the average crystallite size (nm) and  $\rho$  as the alloy density ( $\text{g cm}^{-3}$ ).  $\rho$  was determined by considering that  $\rho_{\text{Pt-Ru}} \text{ (g cm}^{-3}\text{)} = \rho_{\text{Pt}} X_{\text{Pt}}^m + \rho_{\text{Ru}} X_{\text{Ru}}^m$ , with  $\rho_{\text{Pt}} = 21.4 \text{ g cm}^{-3}$  and  $\rho_{\text{Ru}} = 12.3 \text{ g cm}^{-3}$  and  $X_{\text{Pt}}^m$  and  $X_{\text{Ru}}^m$  as the weight percentage of Pt and Ru, respectively.

Catalyst	Metal Content, wt %	Pt:Ru Atomic Ratio	Crystallite and Particle Size, nm		Lattice Parameter, Å	Metal Surface Area, $\text{m}^2 \text{ g}^{-1}$
			XRD	TEM		
Pt/gCMK-3-R2-BM	20	—	5.9	$3.9 \pm 1.3$	3.923	47
Pt/gCMK-3-R2-FAM	22	—	3.7	$3.2 \pm 1.0$	3.926	76
Pt/gCMK-3-R8-BM	16	—	5.6	$4.1 \pm 1.4$	3.920	50
Pt/gCMK-3-R8-EG	24	—	6.2	$5.9 \pm 1.4$	3.919	45
Pt/gCMK-3-R8-FAM	23	—	4.1	$4.9 \pm 1.6$	3.920	68
Pt/C E-TEK	20	—	3.0	—	3.921	93
Pt-Ru/gCMK-3-R2-FAM	26	53:47	6.6	$5.2 \pm 2.3$	3.896	49
Pt-Ru/gCMK-3-R8-EG	22	67:33	3.6	$6.7 \pm 2.8$	3.921	85
Pt-Ru/gCMK-3-R8-FAM	24	55:45	5.6	$3.9 \pm 1.3$	3.898	57
Pt-Ru/C E-TEK	20	45:55	4.4	—	3.866	76



**Figure 1.** XRD patterns of the Pt catalysts supported on gCMK-3s and the commercial Pt/C from E-TEK.

The crystallite sizes were calculated from the (220) reflection, and the values are reported in Table 1 [21]. For the Pt catalysts, the smallest crystallite sizes were obtained for the FAM method and the largest ones for the EG, whereas the opposite was observed for the Pt–Ru materials. This result is in agreement with that reported by Calderón et al. for Pt–Ru catalysts supported on carbon nanofibers and prepared by different synthesis routes [21]. In general, the addition of Ru led to an increase in the crystallite size and thus the metal surface areas (SA) agreeing with the expression described in Table 1. As expected, SA diminished with the increase in the crystallite size, with Pt/gCMK-3-R8-EG displaying the lowest value in the group of the Pt/gCMK-3 catalysts. In the case of Pt–Ru materials, Pt–Ru/gCMK-3-R2-FAM presented lower value in the SA as a consequence of the largest crystallite diameter determined for this material.

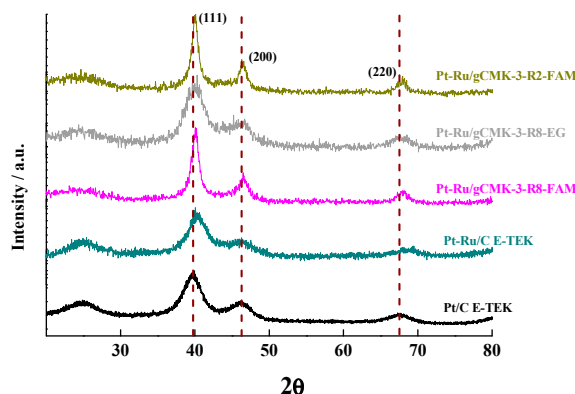


**Figure 2.** XRD patterns of the Pt–Ru catalysts supported on gCMK-3s and the commercial Pt/C and Pt–Ru/C from E-TEK.

Figure 3 shows the TEM images obtained for the Pt/gCMK-3 catalysts, which demonstrate well-dispersed nanoparticles on the carbon support, although some agglomerates can be observed in some cases, such as Pt/gCMK-3-R2-BM and Pt/gCMK-3-R2-EG. Pt/gCMK-3-R2-FAM showed the smallest particle size, while Pt/gCMK-3-R8-EG exhibited the highest one, following the trend observed for the crystallite size values determined by XRD. For the Pt–Ru catalysts (Figure 4), larger particles were observed, especially for Pt–Ru/gCMK-3-R2-FAM and Pt–Ru/gCMK-3-R8-EG. These materials displayed a wide distribution of diameters between 1 and 12 nm, although the catalyst Pt–Ru/gCMK-3-R8-FAM showed a narrower distribution and the smallest particle size among the synthesized Pt–Ru catalysts.

The difference in the magnitude between the crystallite and the particle diameters can be explained as follows: In XRD, an average of the crystallite size is obtained as a consequence of the X-ray beam passing through the crystallites, even if they are agglomerated. During the TEM analysis, a counting and measuring process is performed, which considers dispersed and nonagglomerated crystalline and amorphous particles. Therefore, smaller values are determined [24].

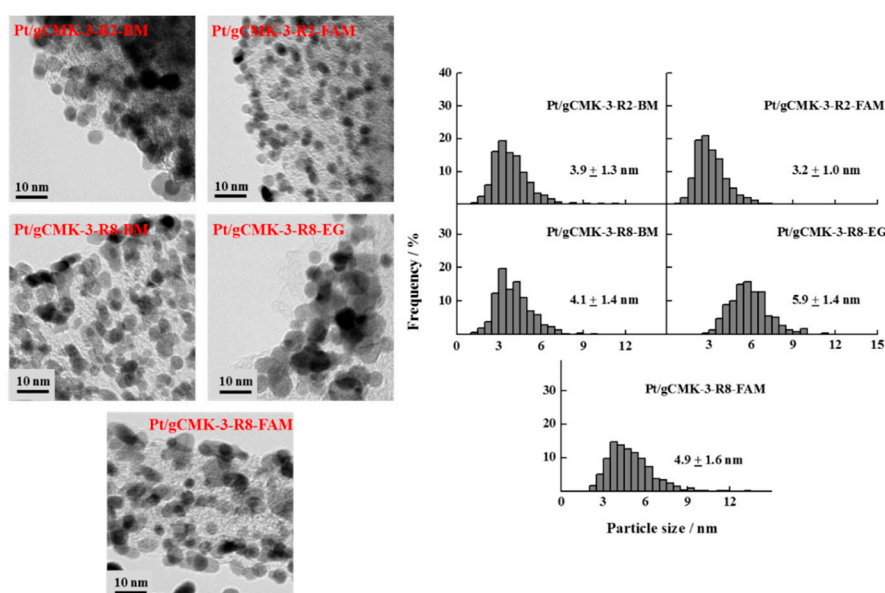


**Figure 3.** TEM images and particle size distributions of the synthesized Pt/gCMK-3 catalysts.



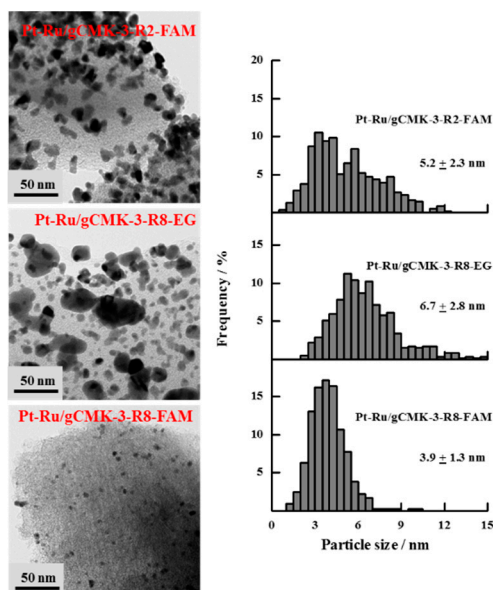


**Figure 4.** TEM images and particle size distributions of the synthesized Pt–Ru/gCMK-3 catalysts.

XPS analysis was carried out to identify the chemical and electronic states of the metals present in the catalysts as well as their relative surface abundance, and the results are reported in Table 2. From the deconvolution of the binding energy spectra of Pt 4f for Pt/gCMK-3 and Pt–Ru/gCMK-3 catalysts, three pairs of Pt peaks were observed, which correspond to the three oxidation states of this metal (see Figure S1 in the Supplementary Information). The transitions generated in the 4f 7/2 and 4f 5/2 orbitals of Pt (0) are described by the peaks close to 71 and 75 eV, while the second and third pair of peaks, located at 73–76 and 75–79 eV, are assigned to Pt (II) and Pt (IV), respectively. In the case of the catalysts Pt/gCMK-3, a similar surface composition of the nanoparticles was observed as all of them displayed a Pt (0) relative surface abundance around 60%. The oxidized states Pt (II) and Pt (IV) exhibited similar abundances between them (close to 20%), indicating that neither the synthesis routes nor the carbon support affect the surface composition of these catalysts. However, in the case of the Pt–Ru/gCMK-3 catalysts (spectra depicted in Figure S2 in the Supplementary Information), several differences were observed in the relative abundance of the Pt surface oxidation states, which are attributed to the entrance of Ru into the Pt lattice that induces changes in the electronic structure and interactions of this metal [25–27]. The catalysts supported on gCMK-3-R8 displayed a higher abundance of Pt (0), a result that matched with the trend observed for the Pt catalysts supported on gCMK-3-R8, which displayed a slightly higher abundance of the Pt (0) oxidation state compared with that observed for the Pt nanoparticles supported on gCMK-R2. Regarding the catalyst Pt–Ru/gCMK-3-R2-FAM, it is possible to conclude that, on this carbon material, the presence of Ru induced the formation of nanoparticles with a high surface content of Pt oxides.

**Table 2.** Electronic and composition parameters of the catalysts supported on gCMK-3s obtained from the XPS data.

Catalyst	Chemical State	Relative Area, %	Binding Energy, eV
Pt/gCMK-3-R2-BM			<i>Pt 4f 7/2</i>
	Metallic Pt	59.4	71.4
	Pt <sup>2+</sup>	21.7	72.6
	Pt <sup>4+</sup>	18.9	75.3
Pt/gCMK-3-R2-FAM			<i>Pt 4f 7/2</i>
	Metallic Pt	60.9	71.4
	Pt <sup>2+</sup>	20.6	72.6
	Pt <sup>4+</sup>	18.5	75.3
Pt/gCMK-3-R8-BM			<i>Pt 4f 7/2</i>
	Metallic Pt	61.1	71.4
	Pt <sup>2+</sup>	19.5	72.6
	Pt <sup>4+</sup>	19.4	75.3
Pt/gCMK-3-R8-EG			<i>Pt 4f 7/2</i>
	Metallic Pt	61.7	71.4
	Pt <sup>2+</sup>	20.1	72.6
	Pt <sup>4+</sup>	18.2	75.4
Pt/gCMK-3-R8-FAM			<i>Pt 4f 7/2</i>
	Metallic Pt	62.1	71.5
	Pt <sup>2+</sup>	18.8	72.7
	Pt <sup>4+</sup>	19.1	75.5
Pt–Ru/gCMK-3-R2-FAM			<i>Pt 4f 7/2</i>
	Metallic Pt	28.7	71.4
	Pt <sup>2+</sup>	17.4	72.6
	Pt <sup>4+</sup>	53.9	74.2
			<i>Ru 3p 3/2</i>
	Metallic Ru	14.9	461.0
	Ru <sup>4+</sup>	27.9	463.2
	Ru <sup>4+</sup> hydrate	57.2	465.4
Pt–Ru/gCMK-3-R8-EG			<i>Pt 4f 7/2</i>
	Metallic Pt	59.1	71.4
	Pt <sup>2+</sup>	22.2	72.7
	Pt <sup>4+</sup>	18.7	75.7
			<i>Ru 3p 3/2</i>
	Metallic Ru	43.6	461.6
	Ru <sup>4+</sup>	18.6	463.2
	Ru <sup>4+</sup> hydrate	37.8	465.3
Pt–Ru/gCMK-3-R8-FAM			<i>Pt 4f 7/2</i>
	Metallic Pt	63.5	71.6
	Pt <sup>2+</sup>	19.2	72.9
	Pt <sup>4+</sup>	17.28	75.4
			<i>Ru 3p 3/2</i>
	Metallic Ru	18.9	461.1
	Ru <sup>4+</sup>	40.7	463.3
	Ru <sup>4+</sup> hydrate	40.4	465.1

Table 2 also reports the results related to the XPS analysis of Ru and its signals. The studied transitions correspond to the 3p orbitals located between 450 and 494 eV (see Figure S3 in the Supplementary Information). A doublet attributed to 3p 1/2 and 3p 3/2 transitions from Ru (0) around 461 and 483 eV was determined, besides two doublets around 463–485 and 465–487, assigned to the transitions of Ru (IV) and hydrated Ru (IV), respectively. The deconvolution analysis suggests an influence of the synthesis method on the Ru oxides surface abundance as the catalysts reduced



with formic acid (FAM) exhibited higher Ru (IV) abundances than that observed for the catalyst reduced with ethylene glycol. This means that the obtaining of different relative abundances for the Ru oxidation states depends on the employed reducing agent, with formic acid leading a less complete reduction of Ru and ethylene glycol promoting a major reduction of Ru.

### 3.2. CO Stripping

The activity of the catalysts toward the carbon monoxide electro-oxidation was evaluated, and the results are depicted in Figures 5 and 6. Pt/gCMK-3-R8 samples exhibited lower onset potential (values between 0.52–0.61-V) than those supported on gCMK-3-R2 (0.63–0.67 V), indicating that linearly adsorbed CO is promoted on these materials due to the high content of metallic Pt in these catalysts, which was detected by XPS (see Table 2) [28]. From this analysis, it is possible to conclude that CO oxidation starts at low potentials on catalysts with a high metallic Pt abundance. Regarding the CO peak potentials, all the Pt samples exhibited a main oxidation peak value around 0.80–0.83 V vs. RHE, similar to that observed for the commercial Pt/C. However, Pt/gCMK-3-R8-EG and Pt/gCMK-3-R8-FAM displayed an additional peak at 0.71 V vs. RHE, indicating a higher ability of the materials supported on gCMK-3-R8 to oxidize the adsorbed CO and thus suggesting an improved tolerance of these materials toward this intermediate formed during the methanol oxidation [21].

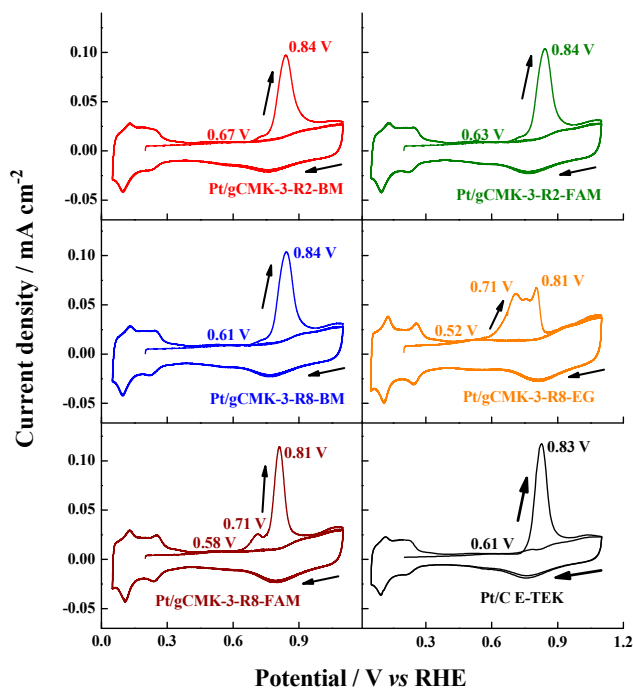


**Figure 5.** Cyclic voltammograms for the  $\text{CO}_{\text{ad}}$  oxidation in 0.5 M  $\text{H}_2\text{SO}_4$  aqueous solution on the Pt/gCMK-3 catalysts. Experiments were performed at  $0.020 \text{ V s}^{-1}$  and  $20^\circ\text{C}$ . CO adsorption potential: 0.2 V vs. reversible hydrogen electrode (RHE).

As expected, the Pt–Ru catalysts oxidized CO at lower potentials than the Pt catalysts (Figure 6) due to the presence of Ru, which helps to oxidize the CO adsorbed on Pt [21]. These values were between 0.43 and 0.47 V compared with 0.50 V detected for the commercial Pt–Ru/C from E-TEK. For the Pt–Ru samples, the main oxidation peak was attained at around 0.54–0.57 V vs. RHE, slightly lower than the commercial one (0.60 V). Only the Pt–Ru/gCMK-3-R8-FAM sample showed an additional peak at lower potential (0.49 V), which could be interpreted as enrichment of Pt and Ru oxides on the surface of the catalyst as this catalyst displayed the highest metallic Pt abundance and also a high presence of Ru oxides [21,29]. This argument is also valid for explaining the positive CO

onset and peak potential values observed for the catalyst Pt–Ru/gCMK-3-R8-EG, which also exhibited the lowest Ru oxides abundance values (see Table 2).

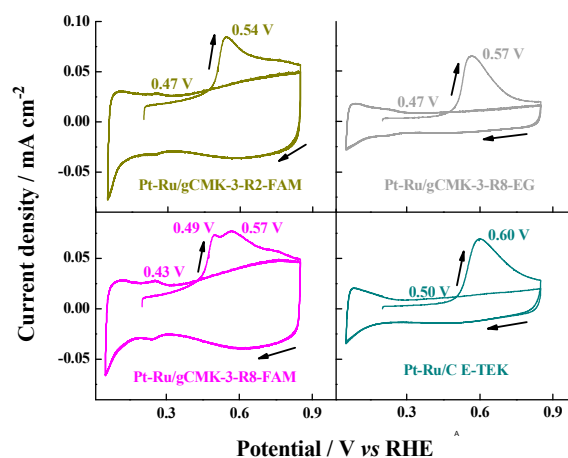


**Figure 6.** Cyclic voltammograms for the  $\text{CO}_{\text{ad}}$  oxidation in 0.5 M  $\text{H}_2\text{SO}_4$  aqueous solution on the Pt–Ru/gCMK-3 catalysts. Experiments were performed at  $0.020 \text{ V s}^{-1}$  and  $20^\circ\text{C}$ . CO adsorption potential: 0.2 V vs. RHE.

These results suggest a positive effect of the use of gCMK-3 carbons on the CO oxidation reaction, which could be attributed to its enhanced diffusion through the gCMK-3 ordered mesoporous structure and a good electronic transfer between the nanoparticles and the support, as already proposed by Calvillo et al. for a Pt catalyst supported on gCMK-3. The mentioned authors reported a significant decrease in these values compared with a commercial Pt/C catalyst from E-TEK, a result explained by the changes in the electronic structure of the metal due to its interaction with the carbon support [6]. On the other hand, the graphitization of the carbon supports did not improve the catalytic activity toward the CO electrochemical oxidation as more positive potential values for the oxidation of this adsorbate were observed compared with those reported for catalysts supported on non-graphitized CMK materials [30]. At the same time, this result matches those found in Reference [6], which were attributed to a lack of surface oxygen groups, which play a key role in the oxidation of this adsorbate.

### 3.3. Methanol Oxidation

Figure 7 shows the behavior of the Pt catalysts supported on gCMK-3s toward the methanol oxidation. The catalysts supported on gCMKs developed significantly higher current densities than the commercial Pt/C. Moreover, the magnitude of the current densities were higher than those reported by Salgado et al. for the oxidation of this fuel on non-graphitized CMK-3-supported Pt and Pt–Ru catalysts [30]. Our results match with those reported in Reference [6], which can be explained by the enhanced electrical conductivity of gCMK-3, which promotes the obtaining of increased current densities for the methanol oxidation.

All the samples showed a methanol oxidation current hysteresis, which has recently been explained by a change in the rate determining step, from water dissociation to the methanol dehydrogenation step. In the forward scan, oxygenated species are adsorbed on the electrode, changing the surface nature of the electrode and thus generating a peak in the backward scan at different potentials attributed to the oxidation of fresh methanol adsorbed on the Pt surface [31,32]. Among the studied catalysts, only Pt/gCMK-R8-BM demonstrated a high oxophilicity as the peak current in the forward scan,  $I_f$ , was higher than that of the backward scan,  $I_b$  [32], while the catalyst supported on gCMK-3-R2 and Pt/gCMK-R8-EG and Pt/gCMK-R8-FAM developed a higher peak current during the backward scan, indicating lower oxophilicity of these materials that improved the adsorption of methanol on the oxidized Pt surface, allowing its oxidation on oxidized Pt active sites [31].

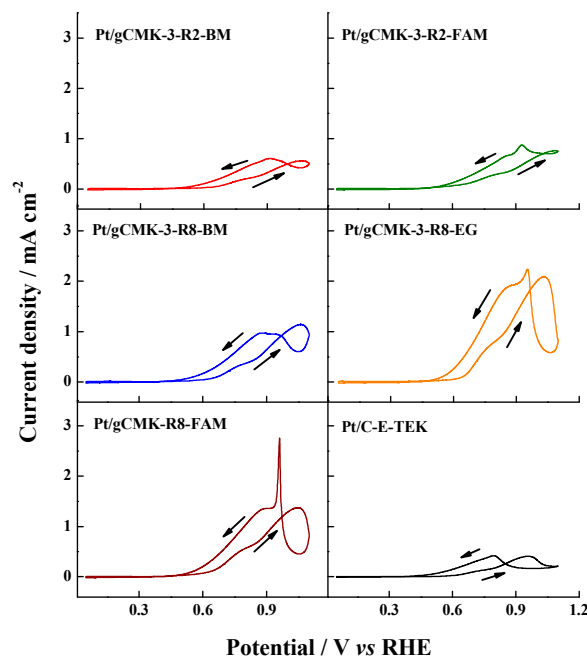


**Figure 7.** Cyclic voltammograms in 2 M  $\text{CH}_3\text{OH}$  + 0.5 M  $\text{H}_2\text{SO}_4$  aqueous solution on the Pt/gCMK-3 catalysts. Experiments were performed at  $0.020 \text{ V s}^{-1}$  and  $20^\circ\text{C}$ .

Similar results were observed for the Pt–Ru catalysts. The catalysts reduced with formic acid showed higher current densities than the commercial Pt–Ru/C and the catalyst reduced with ethylene glycol (see Figure 8). The best performance was obtained with Pt–Ru/gCMK-3-R8-FAM, which can again be related to the high content of Ru oxides in these catalysts, which promote the CO oxidation [21].

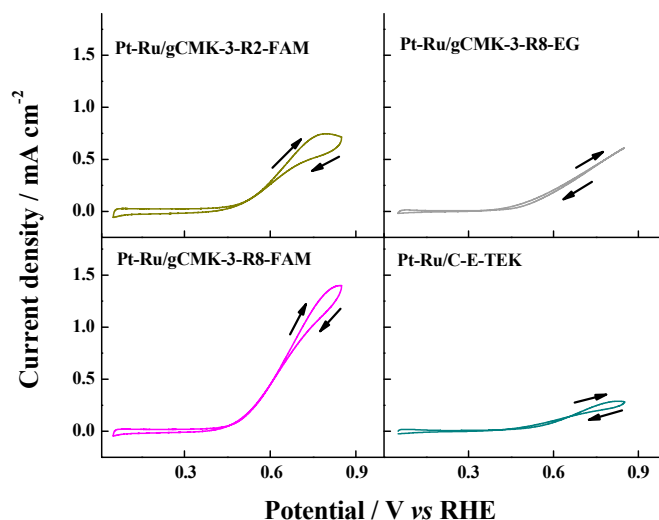


**Figure 8.** Cyclic voltammograms in 2 M  $\text{CH}_3\text{OH}$  + 0.5 M  $\text{H}_2\text{SO}_4$  aqueous solution on the Pt–Ru/gCMK-3 catalysts. Experiments were performed at  $0.020 \text{ V s}^{-1}$  and  $20^\circ\text{C}$ .

Figure 9a depicts the  $j$ – $t$  curves for the methanol oxidation on the Pt and Pt–Ru catalysts supported on graphitized ordered mesoporous carbons recorded at 0.6 V vs. RHE, a typical DMFC work potential. In the case of the Pt catalysts, the commercial one presented the highest current densities, a fact explained by an improved reoxidation of the intermediate species formed during the methanol oxidation, which could be favored by the presence of the micropores of the carbon black, which delays their diffusion and allows their reoxidation [33]. Nevertheless, the difference in the stationary

current densities among the commercial catalyst and the gCMK-3-supported catalyst with the highest performance (Pt/gCMK-3-R8-EG) was around  $11\text{--}12\ \mu\text{A cm}^{-2}$ , low values that allowed us to conclude that the use of Pt/gCMK-3 catalysts could still be an alternative as anodes in DMFCs. Among the synthesized catalysts, no significant differences in the magnitude of the stationary current densities were found, except in the case of the catalyst Pt/gCMK-3-R2-BM, which displayed the lowest current density ( $0.0279\ \text{mA cm}^{-2}$ ).

The behavior of the stationary current densities for the Pt–Ru catalysts was different to that observed for the Pt materials, as can be seen in Figure 9b. The synthesized catalysts developed higher current densities than those observed for the commercial Pt–Ru/C catalyst from E-TEK and the studied Pt catalysts, making evident the effect of Ru and their surface oxides determined by XPS analysis on the enhancement of the methanol oxidation stationary current densities obtained on these catalysts, with Pt–Ru/gCMK-3-R8-FAM being the catalyst displaying the highest stationary current density, as previously observed in the cyclic voltammetry experiments.

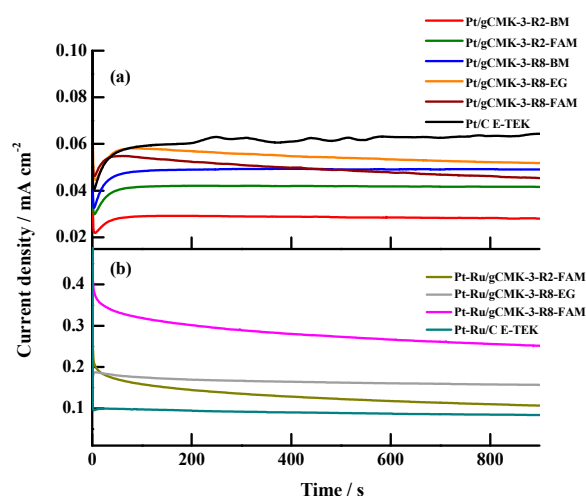


**Figure 9.**  $j$ – $t$  curves in  $2\ \text{M CH}_3\text{OH} + 0.5\ \text{M H}_2\text{SO}_4$  aqueous solution at  $0.60\ \text{V vs. RHE}$  on the Pt/gCMK-3 (a) and Pt–Ru/gCMK-3 (b) catalysts.

Considering the results presented here, it is possible to establish a comparison between the performance of the catalysts presented in this work and those reported for materials supported on ordered mesoporous carbons. In the case of Pt catalysts supported on ordered mesoporous carbons, Su et al. prepared materials using sodium borohydride as reducing agent, obtaining catalysts that achieved current densities close to  $1.6\ \text{mA cm}^{-2}$ , surpassing the values generated for a commercial Pt/C catalyst from E-TEK [34]. The authors explained this high performance by the improved transport of methanol toward the catalytic nanoparticles through the pores of the support. As mentioned above, Salgado et al. [30] synthesized Pt catalysts supported on ordered mesoporous carbons, which displayed CO oxidation peak potentials and methanol oxidation current densities comparable to those presented in this work. The improved diffusion of the electroactive species through the carbon support was stated as the main cause for the remarkable performance of these catalysts. It is important to highlight that the results presented here are quite similar to those described in Reference [6], although in this case, the Pt nanoparticles were supported on graphitized ordered mesoporous carbons. This fact corroborates that the materials studied here possess a catalytic activity that follows the trend of the catalysts already reported in the literature.

The behavior Pt–Ru catalysts supported on ordered mesoporous carbons toward the methanol oxidation have also been studied. Salgado et al. [30] reported the activity of Pt–Ru catalysts supported on non-graphitized ordered mesoporous carbons, which displayed lower methanol oxidation current densities than those reported by Calvillo et al. [6] as well as that obtained in the present study. The increased current densities obtained on graphitized CMK-3 can be explained by the high conductivity

of these materials achieved after the heat treatment applied on them. Other OMCs have been demonstrated to play a key role in the increase in the performance of the as-supported nanoparticles. Maiyalagan et al. compared the activity of highly stable Pt–Ru nanoparticles supported on ordered mesoporous carbons and carbon blacks, finding higher current densities for the methanol oxidation on the OMC-supported materials [35]. Nitrogen doping of ordered mesoporous carbons has also been suggested as an alternative to improve the performance of Pt–Ru catalysts, generating methanol oxidation current densities higher than  $6 \text{ mA cm}^{-2}$  in acidic and alkaline media, which were attributed to both the presence of nitrogen as dopant and the increase in the porosity of the carbon supports as a consequence of the treatment employed to dope the ordered mesoporous carbons [36]. From the comparisons presented here, it is possible to suggest that the Pt and Pt–Ru catalysts supported on graphitized CMK-3 are suitable materials to be employed as anode catalysts in DMFCs. However, further studies are necessary to fully understand and characterize the mechanism of methanol oxidation on these catalysts and therefore finding the effect of carbon support and composition of the catalysts on this reaction. Studies at different temperatures can be useful to determine the rate determining step on the different catalysts, along with differential electrochemical mass spectrometry to identify the onset potentials for both CO and methanol oxidations.

#### 4. Conclusions

Pt and Pt–Ru catalysts supported on graphitized ordered mesoporous carbons (gCMK-3) were synthesized using sodium borohydride, formic acid, and ethylene glycol as reducing agents. Metal contents close to 20 wt% and Pt:Ru atomic ratios close to 1:1 were obtained with well-dispersed metal nanoparticles on the carbon materials and a narrow particle size distribution around 5 nm. The Pt/gCMK-3 catalysts displayed similarities in terms of the surface relative abundance for Pt (0), Pt (II), and Pt (IV) oxidation states, with values near 60%, 20%, and 20%, respectively. On the other hand, the Pt–Ru/gCMK-3 materials exhibited a higher abundance of surface Pt and Ru oxides. As expected, the Pt–Ru materials were the most tolerant to CO as they were able to oxidize this adsorbate at the lowest potentials, an effect attributed to the presence of Ru oxides present on the surface of the catalyst. In agreement with the CO oxidation results, the Pt–Ru catalysts, in particular the one supported on gCMK-3-R8, were the most active ones toward the methanol oxidation. Pt/gCMK-3 catalysts displayed oxidation current densities with some hysteresis, indicating the adsorption of methanol on oxidized Pt to react on this surface. Moreover, the stationary current densities at 0.6 V developed by the Pt–Ru/gCMK-3 catalysts were higher than those of the Pt materials, suggesting a profitable effect of this metal and their oxides on these catalysts. The results found in this research indicate that the studied catalysts can be good candidates to be used as anodes in direct methanol fuel cells.

**Supplementary Materials:** The following are available online at <http://www.mdpi.com/2571-9637/2/1/1/s1>, Figure S1: Pt 4f XPS spectra for the synthesized Pt/gCMK-3 catalysts. Red line: Pt (0), blue line: Pt (II), green line: Pt (IV), black dotted line: fitted curve, black full line: spectrum. Figure S2: Pt 4f XPS spectra for the synthesized Pt–Ru/gCMK-3 catalysts. Red line: Pt (0), blue line: Pt (II), green line: Pt (IV), black dotted line: fitted curve, black full line: spectrum. Figure S3: Ru 3p XPS spectra for the synthesized Pt–Ru/gCMK-3 catalysts. Red line: Ru (0), blue line: Ru (IV), green line: Ru (IV) hydrated, black dotted line: fitted curve, black full line: spectrum.

**Author Contributions:** J.C.C.G. performed the experiments and wrote the paper. V.C. and L.C. synthesized the carbon supports, prepared the catalysts, and performed the physical characterization (EDX, XRD, TEM). D.S. performed the XPS experiments and analysis. R.M. and M.J.L.E. contributed reagents/materials/analysis tools. All the authors conceived and designed the experiments and revised the manuscript.

**Funding:** This work was carried out with the support of the Conversion Group of Gobierno de Aragon T06 and FEDER.

**Acknowledgments:** V.C. kindly thanks the UK Catalysis Hub for resources and support provided via the membership of the UK Catalysis Hub Consortium and funded by EPSRC (EPSRC grants EP/K014706/1 and EP/K014714/1).

**Conflicts of Interest:** The authors declare no conflict of interest.

## References

1. Lu, A.; Schüth, F. Nanocasting: A Versatile strategy for creating nanostructured porous materials. *Adv. Mater.* **2006**, *18*, 1793–1805. [\[CrossRef\]](#)
2. Joo, S.H.; Choi, S.J.; Oh, I.; Kwak, J.; Liu, Z.; Terasaki, O.; Ryoo, R. Ordered nanoporous arrays of carbon supporting high dispersions of platinum nanoparticles. *Nature* **2001**, *412*, 169–172. [\[CrossRef\]](#) [\[PubMed\]](#)
3. Calvillo, L.; Lázaro, M.J.; García-Bordejé, E.; Moliner, R.; Cabot, P.L.; Esparbé, I.; Pastor, E.; Quintana, J.J. Platinum supported on functionalized ordered mesoporous carbon as electrocatalyst for direct methanol fuel cells. *J. Power Sources* **2007**, *169*, 59–64. [\[CrossRef\]](#)
4. Salgado, J.R.C.; Quintana, J.J.; Calvillo, L.; Lázaro, M.J.; Cabot, P.L.; Esparbé, I.; Pastor, E. Carbon monoxide and methanol oxidation at platinum catalysts supported on ordered mesoporous carbon: The influence of functionalization of the support. *Phys. Chem. Chem. Phys.* **2008**, *10*, 6796–6806. [\[CrossRef\]](#) [\[PubMed\]](#)
5. Lei, Z.; An, L.; Dang, L.; Zhao, M.; Shi, J.; Bai, S.; Cao, Y. Highly dispersed platinum supported on nitrogen-containing ordered mesoporous carbon for methanol electrochemical oxidation. *Microporous Mesoporous Mater.* **2009**, *119*, 30–38. [\[CrossRef\]](#)
6. Calvillo, L.; Celorrio, V.; Moliner, R.; García, A.B.; Camean, I.; Lázaro, M.J. Comparative study of Pt catalysts supported on different high conductive carbon materials for methanol and ethanol oxidation. *Electrochim. Acta* **2013**, *102*, 19–27. [\[CrossRef\]](#)
7. Eftekhari, A.; Fan, Z. Ordered mesoporous carbon and its applications for electrochemical energy storage and conversion. *Mater. Chem. Front.* **2017**, *1*, 1001–1027. [\[CrossRef\]](#)
8. Fulvio, P.F.; Mayes, R.T.; Wang, X.; Mahurin, S.M.; Bauer, J.C.; Presser, V.; McDonough, J.; Gogotsi, Y.; Dai, S. “Brick-and-mortar” self-assembly approach to graphitic mesoporous carbon nanocomposites. *Adv. Funct. Mater.* **2011**, *21*, 2208–2215. [\[CrossRef\]](#)
9. Kim, C.H.; Lee, D.K.; Pinnavaia, T.J. Graphitic mesostructured carbon prepared from aromatic precursors. *Langmuir* **2004**, *20*, 5157–5159. [\[CrossRef\]](#)
10. Lee, K.; Ji, X.; Rault, M.; Nazar, L. Simple synthesis of graphitic ordered mesoporous carbon materials by a solid-state method using metal phthalocyanines. *Angew. Chem.* **2009**, *48*, 5661–5665. [\[CrossRef\]](#)
11. Fuertes, A.B.; Alvarez, S. Graphitic mesoporous carbons synthesised through mesostructured silica templates. *Carbon* **2004**, *42*, 3049–3055. [\[CrossRef\]](#)
12. Tang, J.; Wang, T.; Sun, X.; Guo, Y.; Xue, H.; Guo, H.; Liu, M.; Zhang, X.; He, J. Effect of transition metal on catalytic graphitization of ordered mesoporous carbon and Pt/metal oxide synergistic electrocatalytic performance. *Microporous Mesoporous Mater.* **2013**, *177*, 105–112. [\[CrossRef\]](#)
13. Nettelroth, D.; Schwarz, H.C.; Burblies, N.; Guschanski, N.; Behrens, P. Catalytic graphitization of ordered mesoporous carbon CMK-3 with iron oxide catalysts: Evaluation of different synthesis pathways. *Phys. Status Solidi A* **2016**, *213*, 1395–1402. [\[CrossRef\]](#)
14. Sultana, K.N.; Fadhel, A.L.; Deshmane, V.G.; Ilias, S. Novel method for synthesis of electrocatalyst via catalytic graphitization of ordered mesoporous carbon for PEMFC application. *Sep. Sci. Technol.* **2018**, *53*, 1948–1956. [\[CrossRef\]](#)
15. Celorrio, V.; Sebastián, D.; Calvillo, L.; García, A.B.; Fermín, D.J.; Lázaro, M.J. Influence of thermal treatments on the stability of Pd nanoparticles supported on graphitised ordered mesoporous carbons. *Int. J. Hydrog. Energy* **2016**, *41*, 19570–19578. [\[CrossRef\]](#)
16. Rivera Gavidia, L.M.; García, G.; Celorrio, V.; Lázaro, M.J.; Pastor, E. Methanol tolerant Pt<sub>2</sub>CrCo catalysts supported on ordered mesoporous carbon for the cathode of DMFC. *Int. J. Hydrog. Energy* **2016**, *41*, 19645–19655. [\[CrossRef\]](#)
17. Calvillo, L.; Celorrio, V.; Moliner, R.; Cabot, P.L.; Esparbé, I.; Lázaro, M.J. Control of textural properties of ordered mesoporous materials. *Microporous Mesoporous Mater.* **2008**, *116*, 292–298. [\[CrossRef\]](#)
18. Lázaro, M.J.; Calvillo, L.; Bordejé, E.G.; Moliner, R.; Juan, R.; Ruiz, C.R. Functionalization of ordered mesoporous carbons synthesized with SBA-15 silica as template. *Microporous Mesoporous Mater.* **2007**, *103*, 158–165. [\[CrossRef\]](#)
19. Wang, X.; Hsing, I.M. Surfactant stabilized Pt and Pt alloy electrocatalyst for polymer electrolyte fuel cells. *Electrochim. Acta* **2002**, *47*, 2981–2987. [\[CrossRef\]](#)
20. Warren, B.E. *X-ray Diffraction*, 1st ed.; Addison-Wesley: Reading, UK, 1969; pp. 27–40. ISBN 0486663175.



21. Calderón, J.C.; García, G.; Calvillo, L.; Rodríguez, J.L.; Lázaro, M.J.; Pastor, E. Electrochemical oxidation of CO and methanol on Pt–Ru catalysts supported on carbon nanofibers: The influence of synthesis method. *Appl. Catal. B-Environ.* **2015**, *165*, 676–686. [[CrossRef](#)]
22. Calderón, J.C.; Mahata, N.; Pereira, M.F.R.; Figueiredo, J.L.; Fernandes, V.R.; Rangel, C.M.; Calvillo, L.; Lázaro, M.J.; Pastor, E. Pt–Ru catalysts supported on carbon xerogels for PEM fuel cells. *Int. J. Hydrog. Energy* **2012**, *37*, 7200–7211. [[CrossRef](#)]
23. Sebastián, D.; Calderón, J.C.; González-Expósito, J.A.; Pastor, E.; Martínez-Huerta, M.V.; Suelves, I.; Moliner, R.; Lázaro, M.J. Influence of carbon nanofiber properties as electrocatalyst support on the electrochemical performance for PEM fuel cells. *Int. J. Hydrog. Energy* **2010**, *35*, 9934–9942. [[CrossRef](#)]
24. Calderón, J.C.; Ndzuzo, L.; Bladergroen, B.J.; Pasupathi, S. Oxygen reduction reaction on Pt–Pd catalysts supported on carbon xerogels: Effect of the synthesis method. *Int. J. Hydrog. Energy* **2018**, *43*, 16881–16896. [[CrossRef](#)]
25. Yang, G.; Sun, Y.; Lv, P.; Zhen, F.; Cao, X.; Chen, X.; Wang, Z.; Yuan, Z.; Kong, X. Preparation of Pt–Ru/C as an oxygen-reduction electrocatalyst in microbial fuel cells for wastewater treatment. *Catalysts* **2016**, *6*, 150. [[CrossRef](#)]
26. Ye, F.; Liu, H.; Hu, W.; Zhong, J.; Chen, Y.; Cao, H.; Yang, J. Heterogeneous Au–Pt nanostructures with enhanced catalytic activity toward oxygen reduction. *Dalton Trans.* **2012**, *41*, 2898–2903. [[CrossRef](#)] [[PubMed](#)]
27. Qu, J.; Liu, H.; Ye, F.; Hu, W.; Yang, J. Cage-bell structured Au–Pt nanomaterials with enhanced electrocatalytic activity toward oxygen reduction. *Int. J. Hydrog. Energy* **2012**, *37*, 13191–13199. [[CrossRef](#)]
28. Kim, G.J.; Kwon, D.W.; Hong, S.C. Effect of Pt particle size and valence state on the performance of Pt/TiO<sub>2</sub> catalysts for CO oxidation at room temperature. *J. Phys. Chem. C* **2016**, *120*, 17996–18004. [[CrossRef](#)]
29. Jeon, T.Y.; Lee, K.S.; Yoo, S.J.; Cho, Y.H.; Kang, S.H.; Sung, Y.E. Effect of surface segregation on the methanol oxidation reaction in carbon-supported Pt–Ru alloy nanoparticles. *Langmuir* **2010**, *26*, 9123–9129. [[CrossRef](#)]
30. Salgado, J.R.C.; Alcaide, F.; Álvarez, G.; Calvillo, L.; Lázaro, M.J.; Pastor, E. Pt–Ru electrocatalysts supported on ordered mesoporous carbon for direct methanol fuel cell. *J. Power Sources* **2010**, *195*, 4022–4029. [[CrossRef](#)]
31. Chung, D.Y.; Lee, K.J.; Sung, Y.E. Methanol electro-oxidation on the Pt surface: Revisiting the cyclic voltammetry interpretation. *J. Phys. Chem. C* **2016**, *120*, 9028–9035. [[CrossRef](#)]
32. Fu, X.; Zhao, Z.; Wan, C.; Wang, Y.; Fan, Z.; Song, F.; Cao, B.; Li, M.; Xue, W.; Huang, Y.; et al. Ultrathin wavy Rh nanowires as highly effective electrocatalysts for methanol oxidation reaction with ultrahigh ECSA. *Nano Res.* **2019**, *12*, 211–215. [[CrossRef](#)]
33. Calderón, J.C.; García, G.; Querejeta, A.; Alcaide, F.; Calvillo, L.; Lázaro, M.J.; Rodríguez, J.L.; Pastor, E. Carbon monoxide and methanol oxidations on carbon nanofibers supported Pt–Ru electrodes at different temperatures. *Electrochim. Acta* **2015**, *186*, 359–368. [[CrossRef](#)]
34. Su, F.; Zeng, J.; Bao, X.; Yu, Y.; Lee, J.Y.; Zhao, X.S. Preparation and characterization of highly ordered graphitic mesoporous carbon as a Pt catalyst support for direct methanol fuel cells. *Chem. Mater.* **2005**, *17*, 3960–3967. [[CrossRef](#)]
35. Maiyalagan, T.; Alaje, T.O.; Scott, K. Highly stable Pt–Ru nanoparticles supported on three-dimensional cubic ordered mesoporous carbon (Pt–Ru/CMK-8) as promising electrocatalysts for methanol oxidation. *J. Phys. Chem. C* **2012**, *116*, 2630–2638. [[CrossRef](#)]
36. Sebastián, D.; Nieto-Monge, M.J.; Pérez-Rodríguez, S.; Pastor, E.; Lázaro, M.J. Nitrogen doped ordered mesoporous carbon as support of PtRu nanoparticles for methanol electro-oxidation. *Energies* **2018**, *11*, 831. [[CrossRef](#)]

